Large-scale stiffness tests bounding a deep bedding plane in the Shaftsbury Shales

Colin Dreger[1]
SNC Lavalin Inc., Vancouver, Canada
Vicki Nguyen
Klohn Crippen Berger, Vancouver, Canada
Derek Martin[1], Hossein Rafiei Renani & Garry Stevenson
Klohn Crippen Berger, Vancouver, Canada
Andrew Watson
BC Hydro, Vancouver, Canada
[1]Seconded

GeoCalgary 2022 October 2-5 Reflection on Resources

ABSTRACT
Major structures of the Site C hydroelectric project are founded on the Shaftesbury Shale. The 2010 redesign of these structures on a RCC foundation deepened the excavations to El. 375 m to take advantage of the increasing foundation stiffness with depth. In 2020, pressuremeter testing to El. 340 and two large scale split-lateral load tests between El. 370 and 375 were carried to quantify the foundation stiffness. Loading assemblies for the lateral load tests comprised 2.3 m diameter steel casings with two laterally oriented O-cells installed in drilled shafts. Five SAAs measured rock mass deformations of approximately 1 mm as the lateral loads reached 81 MN. Three dimensional numerical analyses of the load test showed an elastic deformation modulus of approximately 20 GPa gave good agreement with the measured displacements. This modulus value is approximately 4 times greater than the foundation stiffness determined at higher elevations. The analysis also indicated that at the scale of these lateral load tests near horizontal bedding planes in the shale had negligible influence on the stiffness.

RÉSUMÉ
Les principales structures du projet hydroélectrique Site C sont fondées sur les schistes de Shaftesbury. En 2010, la nouvelle conception de ces structures sur une fondation en BCR a approfondi les excavations jusqu'à l'élévation 375 m pour profiter de l'augmentation de la rigidité des fondations en profondeur. En 2020, un essai pressiométrique à l'élévation 340 m et deux essais de chargement latéral à grande échelle entre l'élévation 370 et 375 m ont été réalisés pour quantifier la rigidité de la fondation. L'assemblage utilisé pour les essais de charge latérale comprenait des tubages en acier de 2,3 m de diamètre avec deux cellules Osterberg orientées latéralement et installées dans des puits forés. Cinq SAA ont mesuré des déformations du massif rocheux d'environ 1 mm alors que les charges latérales atteignaient 81 MN. Des analyses numériques tridimensionnelles représentatifs de l'essai de chargement latéral ont montré une bonne corrélation entre le module de déformation élastique (environ 20 GPa) et les déplacements mesurés. Cette valeur du module de déformation est environ 4 fois supérieure à la rigidité de la fondation déterminée à des élévations plus élevées. L'analyse a également indiqué qu'à l'échelle de ces essais, les plans de litage horizontaux dans le schiste avaient une influence négligeable sur la rigidité.

1 INTRODUCTION

The Site C Clean Energy Project currently under construction near Fort St. John, British Columbia, comprises an earthfill dam, spillway structure, and 1,100 MW generating station. The design overview is provided by Watson et al. (2019) and the site layout shown in Figure 1.

The spillway and generating station located on the right bank required a large excavation which was anticipated to generate movements in the shale foundation due to loss of confinement and rebound (Hanna and Little 1991). To mitigate these effects, the structures are being constructed on a roller-compacted concrete (RCC) buttress which replaces the surcharge load on the bedrock foundation and will resist movements along potential weak bedding planes. An RCC shear key with an invert El. 375 was included in the design to deepen this resistance. Additional enhancements to the foundations were adopted during construction to intercept deep bedding planes and reduce the potential for movements associated with swell and valley rebound that are expected to occur over the 100-year design life of the project, but challenging to quantify.

Figure 1. Site C Project Component Configuration

2 GEOTECHNICAL CHARACTERIZATION

The Lower Cretaceous Shaftesbury Formation consists of moderately weak silty shale, with minor beds of siltstone, sandstone, and shale with a northeast dip of approximately 1º. The formation has been subdivided into 14 rock units at the site based largely on major rock type and gradational

changes in successive shale units. The composition and location of these units with respect to the Marl marker bed differ only slightly across the dam site; however, in general the rock on the right bank is comparatively finer grained than that of the left bank (Heidstra et al. 2016).

The Peace River area has seen multiple glaciations during the period of river downcutting. This loading and unloading of the weaker shales have caused many of the geological discontinuities encountered at the site, such as steeply dipping relaxation joints, sheared bedding planes, and cross-cutting sub-horizontal shears. These geological features are discussed by Imrie (1991).

Extensive investigation and testing of the Shaftesbury Formation were initiated in the 1970s when project studies first began. Characterization of the rock mass stiffness and strength was largely completed by the mid-1980s (Cornish & Moore 1985; Sargent & Cornish 1985). Comprehensive laboratory testing programs were conducted, and in-situ testing techniques were employed to determine rock mass strength and stiffness. Testing included Menard pressuremeter tests, plate load tests, biaxial cell tests, large-scale shear tests (Shuri et al. 1984), and a test chamber to investigate rock mass behavior for diversion tunnel construction (Little 1989).

The early characterization campaigns on the right bank focused on the rock mass providing the foundation for the structures in the 1980 design. The 2010 redesign of these structures on a RCC foundation deepened the rock excavations to El. 375 to take advantage of the increasing foundation stiffness with depth. Pressuremeter testing in 2020 to El. 340 and two large scale split-lateral load tests between approximately El. 370 and 375 were carried out to quantify the changes in foundation stiffness.

3 SPLIT-LATERAL TESTS CONFIGURATION

The split-lateral tests have been used on other projects to establish the rock mass response to lateral loading in weak rocks (Brown et al 2018). The primary objectives of the split-lateral tests were to determine the rock mass stiffness and strength at a scale that captures the rock discontinuities including weak bedding planes using a method that minimizes the disturbance to the rock. Two lateral loading assemblies were installed in two 2.6 m diameter test shafts drilled through the RCC and into the shale foundation of the East and West Stilling Basins of the Spillway (Figure 2).

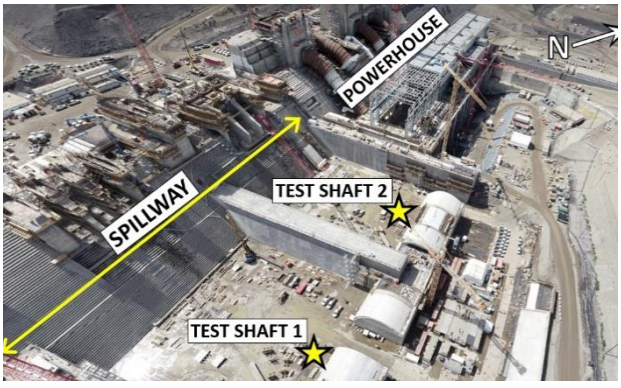

Figure 2. Location of the split-lateral tests in the Spillway.

3.1 Shaft Drilling and Shaft Wall Imaging

Drilling of Test Shafts 1 and 2 commenced on October 19 and 29, 2020, to depths of approximately 43 m using a combination of rock auger, drilling bucket, and coring barrel. RCC was encountered from grade (El. 396.0 m) to a depth of 13.3 m (El. 382.7 m), overlying shale bedrock to the termination of the shaft.

The rate of groundwater ingress into the shafts varied greatly between shafts. Inflow rates in Test Shaft 1 were generally less than 1.5 L/min. Minor seepage into Test Shaft 2 was noted from the RCC; however, considerable groundwater ingress was observed from the RCC-shale interface at El. 382.7 m to roughly El. 373 m. This increase was attributed to shears in the rock mass identified during televiewer logging of the instrumentation holes.

Three different methods of test shaft imaging were utilized for inspection and geological interpretation, including downhole cameras and photogrammetric imaging conducted by Underhill Geomatics Ltd. (Underhill). Sonar profiling was used to determine the shaft dimensions, verticality, and straightness.

Following drilling, the condition of the shaft walls was initially inspected using a shaft inspection camera. The opacity of the water and smeared shale cuttings on the wall precluded useful observations of geological structure. To facilitate geological mapping, the shaft walls were imaged using a 360º camera fitted with LED lighting and photogrammetric processing techniques to produce a 3D shaft model. Figure 3 shows views of Test Shaft 1 and 2 images displaying the observed low angle cross-cutting shears, relaxation joints, siltstone and concretion layers, and bedding planes.

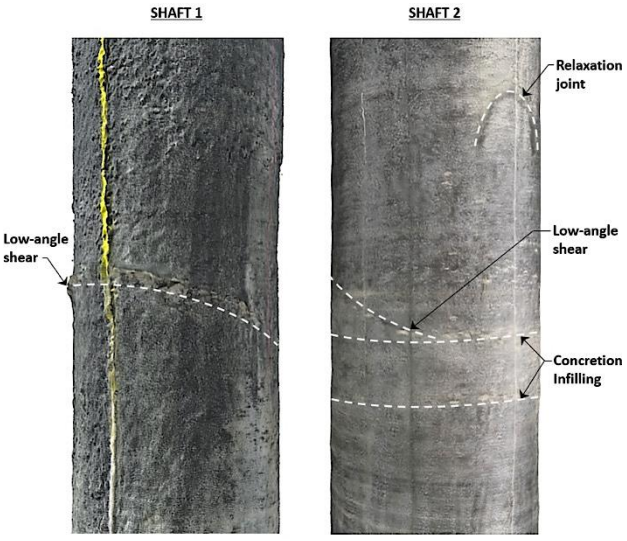

Figure 3. Shaft models generated from photogrammetry

3.2 Loading Assemblies

The loading assemblies were supplied by Fugro Loadtest (Loadtest). The loading assemblies comprised two laterally orientated 26.7 MN tandem O-cells set between diametrically-opposed active and passive segments of a 4.0 m long, 2.3 m diameter steel casing – fundamentally a

large Goodman Jack. The general testing assembly configuration is provided in Figure 4. The active segment had a height of approximately 2.0 m and was pre-filled with concrete (f_c'=35 MPa) before arriving on site. Upper and lower steel confining plates were welded to the assembly above and below the active segment, separated by sheets of Teflon such that the active side was attached solely to the O-cells and frictional resistance of the upper and lower contact surfaces was minimized. The passive segment was the full height of the assembly.

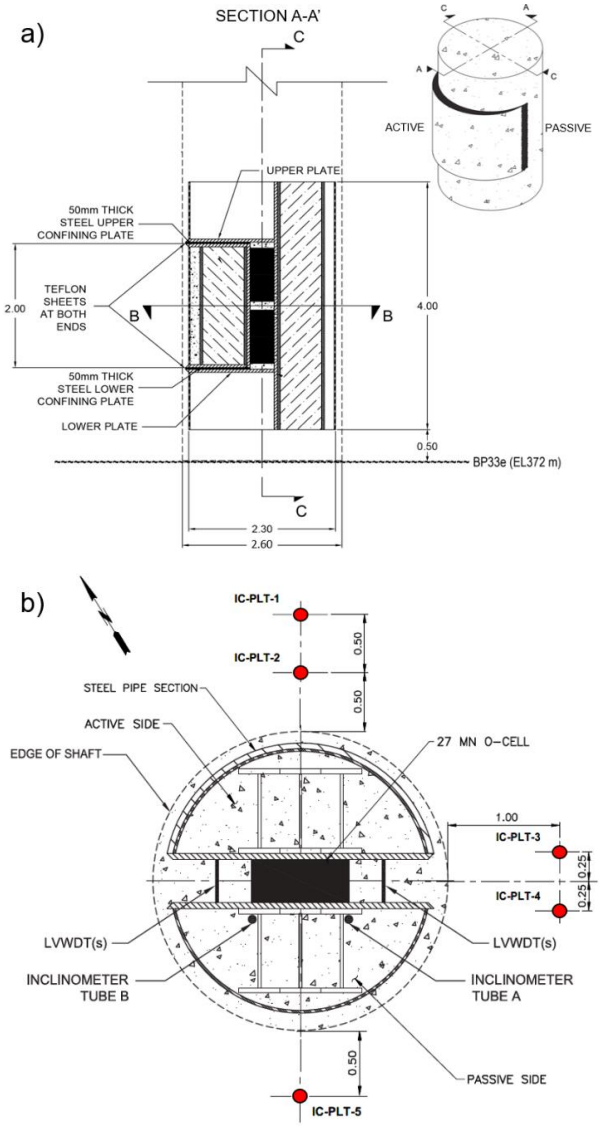

Figure 4. Lateral load assembly (Test Shaft 1; LT-01); a) section view; and b) plan view (units are in metres)

3.3 Testing Instrumentation

In-situ tests are challenging to successfully execute when the deformations are expected to be small and test components are unique. Scoping calculations indicated considerable instrumentation redundancy would be needed to ensure a successful test. Instrumentation was installed around each shaft to monitor the behavior of the rock mass and within the loading assemblies to monitor deformations and loads. Figure 4b provides the general instrumentation configuration used for both tests. Instruments included the following:

- 5 Shape Accelerometer Arrays (SAAs)
- 8 Linear vibrating wire displacement transducers (LVWDTs) installed in the loading assemblies
- 2 In-place inclinometers (IPIs); and
- 1 Vibrating wire piezometers.

Two SAA's were installed in vertical boreholes adjacent to the shafts to monitor deformations in the rock mass on the active loading side and one SAA was installed in the rock mass on the passive side. Two SAA's were also installed in the rock mass where tensile stresses were expected at the boundary between active and passive loading (Figure 4b). One vibrating wire piezometer was installed to monitor porewater pressure on a bedding plane during loading.

Loadtest installed 8 LVWDTs to measure the expansion/contraction of the cells, and two in-place inclinometers (IPI) in the passive sides of the assemblies.

3.4 Lateral Loading Procedure

Test loads were applied incrementally by two O-cells in the assemblies, operated independently using two pumps. The intention was to complete unload-reload loops to explore the elastic response of the rock mass, hold the load at certain increments to determine creep behavior, and continue to load the shale until reaching either the: 1) capacity of the shale; 2) maximum travel of the O-cells (225 mm); or 3) capacity of the loading system.

Pressure to the O-cells, O-cell displacement (via LVWDTs), and lateral deformations of the IPIs were measured by Loadtest during the tests. Sampling of load and LVWDT data was conducted every 10 seconds and every 30 seconds for the IPIs. RST Instruments Ltd. (RST) collected the SAA data.

Testing was initiated by applying sufficient load to break the tack welds (less than 3 MN) which held the O-cells closed during transport and installation, followed by unloading. Load was generally applied in increments of 0.3 MN each minute during the tests. Two unload-reload loops were completed during the loading sequence, followed by loading to the maximum test loads. Unloading was conducted in decrements of 0.5 MN every minute.

Maximum loads of approximately 73 MN and 81 MN were reached during the LT-01 and LT-02 load tests, respectively. The maximum difference in cell load measured between the upper in lower cells 1.3 MN prior to the depressurization event. The maximum difference during the LT-02 test was 2.8 MN. Figure 5 summarizes the applied loading during each test.

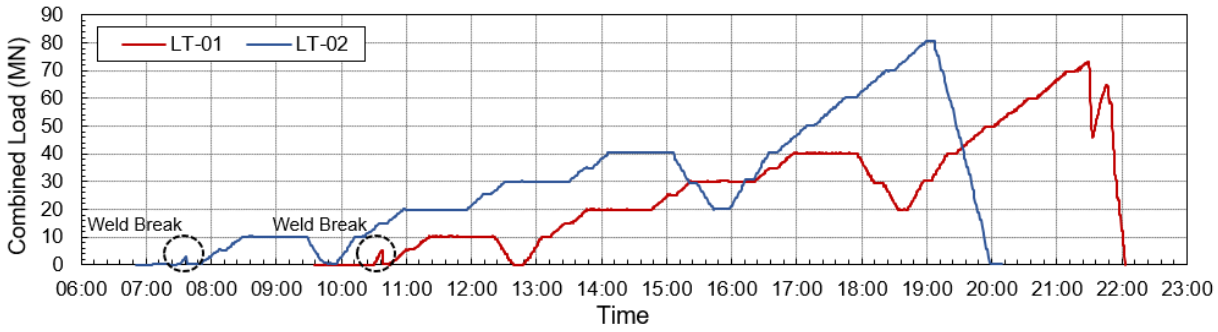

Figure 5. Total combined loads from the upper and lower O-cells over the duration of the tests.

3.5 Loading System Response

Loading assembly deformations were calculated cumulatively from IPI data assuming a 'fixed' level corresponding to a depth of 3 m below grade (El. 393.0 m). During the LT-01 test, a maximum passive-side displacement of 1.3 mm was recorded at an elevation of 373.5 m – the approximate location of the lower O-cell. The average passive-side displacement over the height of the assembly was 0.8 mm.

A maximum passive-side displacement of 1.4 mm was recorded during the LT-02 test at El. 369.0 m. The average passive-side displacement over the height of the assembly was 0.6 mm. Passive direction displacements appeared to be centered in the lower half of the assembly (below El. 370.5 m), with some active direction (negative) displacements observed at the upper cell between elevations of 372.0 m and 370.5 m. Movements in the negative direction were less than 0.4 mm; however, this may indicate that the assembly had a slight rotational tendency.

In general, the LVWDT data was erratic and individual sensors did not accurately represent expansion/retraction of the O-cells. Loadtest combined both LVWDT and IPI data sets and concluded that at the maximum loads lateral displacements were 0.64 mm and 0.76 mm for the active and passive segments, respectively, during the LT-01 test. Displacements of 0.64 mm and 0.62 mm were calculated for the LT-02 test active and passive segments. Active segment displacements were calculated by subtracting averaged LVWDT displacements from the passive displacements measured using the IPIs.

3.6 Testing Summary

In general, the split lateral load tests were completed successfully. The required load-deformation data was obtained, and the objectives were met. The loading assembly displacements measured during the tests were ~1 mm indicating a very stiff rock mass response.

4 ROCK MASS RESPONSE TO LOADING

4.1 Rock Mass Instrumentation Overview

Deformations were measured by the SAAs over their sensorized lengths from grade (El. 396 m) to El. 365 m for IC_PLT1-1 and 2 (full sensorized length) with a 0.25 m node spacing, and from approximately El. 382 m to El. 365 m for IC_PLT1-3 through IC_PLT1-5 with a 0.5 m node spacing.

4.2 Shape Accelerometer Arrays

SAA data was collected at 1-minute intervals using a manual trigger during the 1 and 8-minute hold periods and a data acquisition program set to a 1-minute reading frequency during the 60-minute hold periods.

Examples of the SAA profiles recorded during the LT-01 and LT-02 tests are shown in Figure 6. Sub-millimetre measurements were collected and deformation trends were evident. Variability of the SAA data was assessed using data collected during the one-hour hold periods. The difference between the minimum and maximum readings was less than 0.1 mm below El. 380 m, and error decreased with depth. Manual readings in the active side casings showed the SAA data agreed with the manual readings.

Instruments installed on the active sides showed the direction of resultant movement deviated from the active loading direction by 3º to 7º for LT-01 and 10º to 15º for LT-02. This may be attributed to imperfections in the assemblies or alignments of the assembly and/or SAAs.

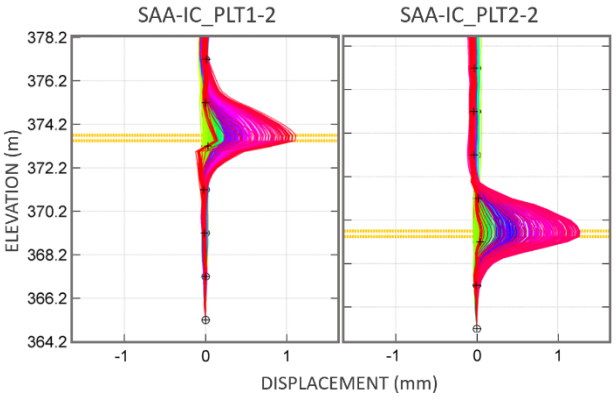

Figure 6. SAA measurements at SAA PLT1-2 and PLT2-2

Active Side

During the LT-01 test, maximum resultant displacements measured on the active side were 0.8 mm and 1.1 mm at IC_PLT1-1 and IC_PLT1-2, respectively, at the maximum load of 72.7 MN. Maximum active side displacements during the LT-02 test were 1.0 mm and 1.3 mm at IC_PLT2-

1 and IC_PLT2-2, at the maximum load of 81.0 MN. Load-deformation measurements for the SAA installed at IC-PLT1-2 are plotted in Figure 7 using a 5-minute moving average to show the data trends more clearly. Loads shown are the combined O-cell loads.

The initial slope of the plot in Figure 7 represents the stiffness of the loading assembly system. After an applied load of approximately 8 to 10 MN and breaking the "tack welds" of the loading assembly, the slope deceases reflecting the rock mass response to loading.

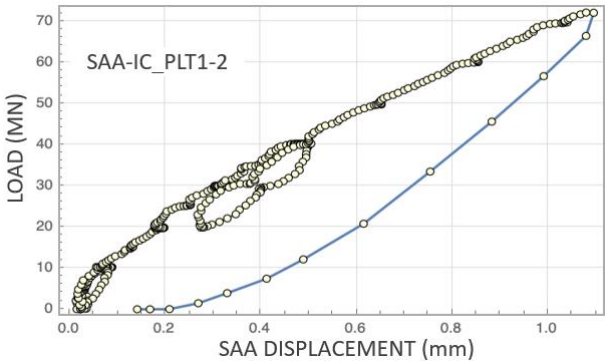

Figure 7. Displacements measured at SAA IC_PLT2

Passive Side

Displacements measured on the passive side at SAAs installed in IC_PLT1-5 and IC_PLT2-5 were approximately 0.9 mm during both tests. Measurements were generally in good agreement with the displacements measured by the IPIs in the passive side of the loading assemblies with some attenuation of displacement toward the SAAs. This indicates effective load transfer to the rock mass and little compressive deformation of the loading assembly and rock mass separating the SAAs and IPIs.

Tensile Side

The maximum displacement measured in the active tensile direction was approximately 0.2 mm at IC_PLT1-3. The other instruments all showed less than 0.1 mm in the active and passive tensile directions.

4.3 Piezometers

Excess porewater pressures measured by PVW_PLT1-2 during the LT-01 test were negligible prior to the 40 MN load and appeared to show erroneous trends during the test. This was likely due to inadequate saturation of the porous stone in the tip. Consequently, the data was disregarded. During the LT-02 test, PVW_PLT2-2 generally appeared to show a good correlation with applied load. Incremental increases and decreases in pressure were apparent during loading and unloading.

5 ROCK MASS PROPERTIES

The 1980's Site C investigations concluded that the isotropic Young's modulus for the shale was E = 4.3 GPa, with an anisotropic modulus of E_h = 6.6 GPa and E_v = 4 GPa. This finding was based on Menard pressuremeter tests and plate load tests carried out from Adit 3 (El. 415). Recent pressuremeter tests conducted in the spillway and powerhouse between El. 390 and El. 340 m by Cambridge Insitu Ltd. (Cambridge InSitu) showed that the Young's modulus increases with depth and ranged from E_h = 8 GPa to a maximum value of E_h = 23 GPa (Conetec 2020).

The rock mass responses measured during the two lateral tests were used to establish the large-scale rock mass stiffness around the 2.6-m-diameter test shafts.

5.1 FLAC3D Back Analysis

A three-dimensional numerical model was developed using the finite-difference geotechnical software FLAC3D to simulate the lateral load tests (Figure 8). The loading assembly was positioned within a 20 m x 20 m x 31 m column consisting of shale between El. 365 m and El. 383 m and RCC from El. 383 m to El. 396 m. To improve the precision of the model in the vicinity of loading, the mesh was refined in a region that extended 2 m above and below the assembly. The mesh representing the shale was scaled radially around the shaft with smaller zones near the edge.

All five SAAs were included in the model as simulated inclinometers. Additional mesh refinement was completed near IC3 and IC4 for both tests since the incremental displacements measured at these instruments were very small (< 0.1 mm).

The lateral loading apparatus was simulated by adding interfaces to permit a section of the assembly to extend outwards. The interfaces above and below the test section were given a normal stiffness of 20 GPa, negligible shear stiffness, and very low frictional strengths (φ = 1°) to represent the Teflon sheeting at these boundaries. The interface along the assembly centerline was assigned a very low frictional strength (φ = 1°) and negligible normal and shear stiffnesses to allow the section to move freely during loading/unloading. Parameters assigned to the model materials are provided in Table 1. This model was run with gravity loading as a total stress analysis for the intact materials and effective stress analysis for frictional interfaces.

To simulate the load applied by the load cells, a surface pressure was applied on the interface along the centerline of the test assembly. This caused the assembly to deflect towards the passive side while the active segment was pushed towards the active side, as shown on Figure 8. The test was simulated by increasing or decreasing the applied pressure in increments following the loading sequence. After each load increment, the model was cycled to equilibrium to calculate the deformation and stress response.

Table 1. Material Parameters

Material	Density (kg/m^3)	Young's Modulus (GPa)	Poiss. Ratio	Friction Angle (°)	Cohesion (MPa)	Tension (MPa)
Shale	2500	Varies[1]	0.3	40	Varies[1]	Varies[1]
RCC	2400	20	0.3	45	2	1
Concrete	2400	41	0.2	45	2	1

[1]Calibrated value

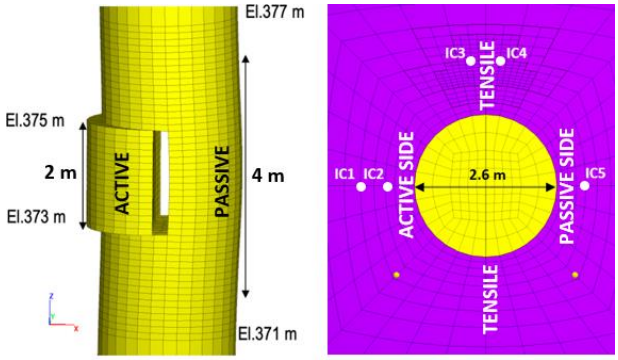

Figure 8. FLAC3D Deformation Model Geometry

5.2 Isotropic Deformation Modulus

The deformation modulus for the shale was estimated by applying different assumptions for the Young's modulus in the model. The shale was initially modeled using the elastic constitutive model with E = 4.3 GPa. This model generated displacements that were significantly higher than were measured during the tests, with a maximum model displacement of 2.8 mm versus 1.1 mm for IC2 (Figure 9).

As demonstrated by the site investigations, the rock mass stiffness increases with depth. Based on compiled pressuremeter and historical test data, the following modulus distribution was adopted for the model:

- Above El. 413 m: E = 4.3 GPa
- El. 413 m to 387 m: E increases from 4.3 to 6.6 GPa
- El. 387 m to 368 m: E increases from 6.6 to 22 GPa
- Below El. 368 m: E = 22 GPa

When the above modulus function was simulated, the displacement reached a maximum value of 0.8 mm for IC2 (Figure 10) which is less than measured. Although the displacements were lower, the slope of the simulated plot was a better fit to the measured displacements up to 0.3 mm during loading. A modulus of E = 18 GPa was calculated at the elevation of maximum displacement (El. 373.74 m). The simulated inclinometer results for this set of parameters are shown on Figure 11 and show a similar shape as the measured data; however, the maximum displacements are generally 0.2 to 0.4 mm lower.

5.3 Anisotropic Modulus

The calibration model was used to investigate the potential anisotropic nature of the shale stiffness. For this model, the "ubiquitous-anisotropic" (UA) constitutive model was applied to the shale. This model was developed to represent a rock-like material that contains weak bedding planes along a given orientation. Two stiffnesses can be applied, one along a discrete plane with a Mohr-Coulomb yield criterion, and one for all other orientations where the material is assumed to behave elastically.

Using the stiffness function derived from the isotropic interpretation in the weak direction, it was determined that an anisotropic stiffness ratio of E_v/E_h = 0.4 yielded the best fit, particularly for IC1. However, it did not significantly impact the load versus displacement response for IC2 at the point of maximum displacement. Overall, the inclusion of stiffness anisotropy helped to improve the shape of the simulated curves (Figure 12); however, it did not have a significant impact on IC2 to IC5 displacements.

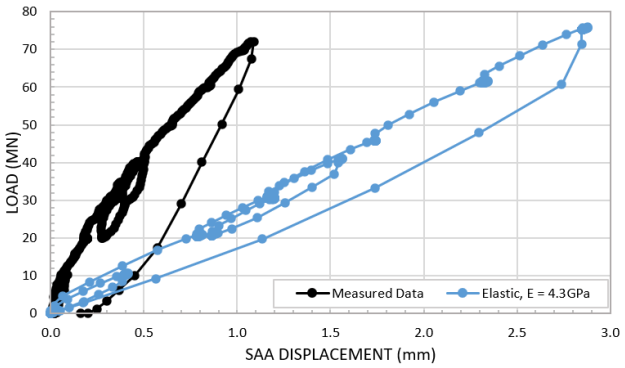

Figure 9. IC2 displacement comparison; E=4.3 GPa

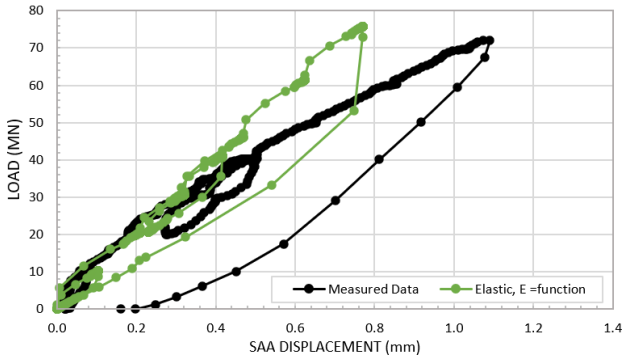

Figure 10. IC2 displacement plot; E= Isotropic function

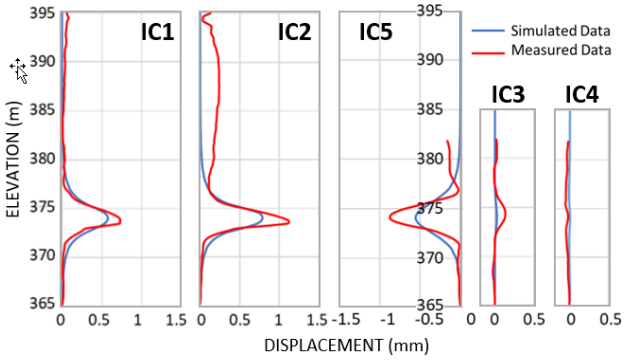

Figure 11. Displacement plots; E= Isotropic function

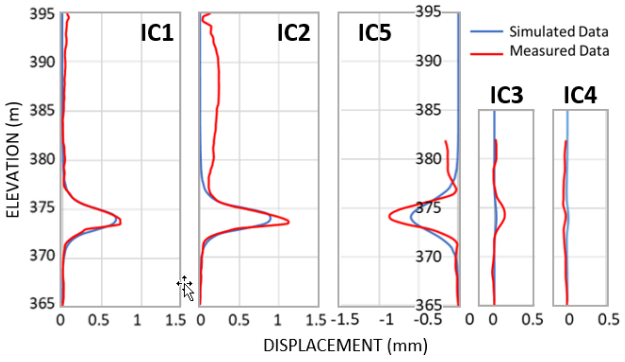

Figure 12. Displacement plots; E= Anisotropic function

5.4 Influence of Bedding Plane Shear

To investigate the influence of a bedding plane shear on the measured displacements, a shear locally referred to as BP33e was positioned 1 m above or below the loading assembly. However, it should be noted no evidence of bedding plane shear displacements was observed at any of the instruments. BP33e was simulated in the deformation model with a frictional strength of φ = 11°. In the deformation model, the response along BP33e is clearly indicated with a flat shear plane in all of the modelled inclinometers (Figure 13). In comparison, the measured responses are generally curved and symmetric about the point of maximum displacement with no obvious preferential movements at the inferred elevation of the bedding plane. These results indicate that loading from the lateral load tests were insufficient to generate bedding plane shear displacements.

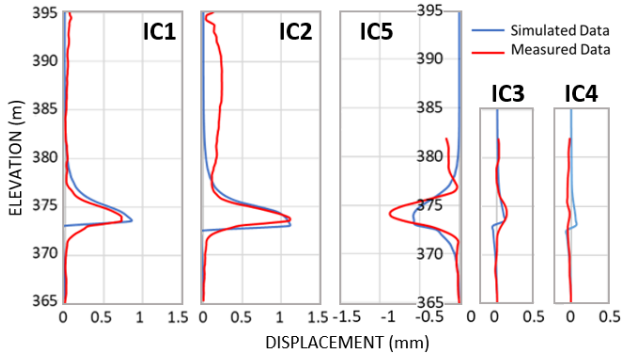

Figure 13. Displacement plots; E= Isotropic function with a bedding plane shear 1 m below the loading assembly

5.5 Shear Strength

The shale shear strength had been estimated from historic triaxial tests using c = 0.25 MPa and φ = 35°. In the 2020 pressuremeter field program, 2 of the 84 pressuremeter tests were classed as “yielding” (Conetec 2020). The two test results where yielding was experienced had estimated shear strengths of c = 0.7 MPa and φ = 43° (partial yielding) and c = 0 MPa and φ = 47° (shear failure).

The load tests created a compressive stress of 16 MPa on the boundary of the rock. Teflon contacts at the active side created shear stress concentrations near the active boundary. To calibrate the shear strength, the cohesive strength was varied, starting at the value of 0.7 MPa. The friction angle for the shale was kept constant at φ = 40° and the isotropic stiffness function was used. A cohesive strength of c = 0.7 MPa increased simulated displacements at IC2 to 50% larger than that which was measured. At c = 1.6 MPa, the simulated model data was in agreement with the measured values during the loading and unloading phases (Figure 14).

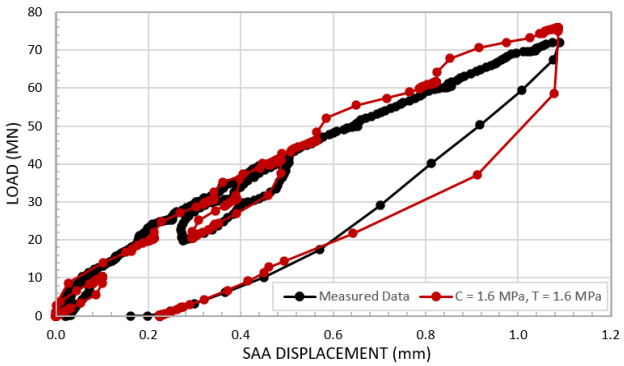

Figure 14. IC displacement plot; c = 1.6 MPa, t = 1.6 MPa

5.6 Tensile Strength

The tensile strength for the shale at the depth of the load tests was unknown. Cambridge InSitu estimated the tensile strength using the pressuremeter tests (ConeTec 2020). In the vicinity of the lateral load tests there were 14 tests between El. 350m and El. 385m. The tensile strengths from those tests ranged from 0.5 MPa to 1.7 MPa with a mean value of 1.0 MPa.

The tensile elastic stress distribution at the maximum test load is shown in Figure 15. When simulating the tensile stresses and strength, a tensile crack forms once the tensile strength is exceeded. The crack length and its opening characteristics are unknown but influence the displacements measured at IC3 and IC4. The reliability of the SAA measurement below 0.1 mm as the load reaches 81 MN increases the uncertainty in the measured data. Using the stiffness function and the best fit cohesive strength, the tensile strength was evaluated by progressively decreasing it below 1.6 MPa. At t = 1.6 MPa, modelled displacements match the IC2 measured data but underpredicts the tensile displacements at IC3 and IC4. At t = 0.8 MPa, model displacements exceeded the measured values at IC3 and IC4 (Figure 16); however, there is little change to IC1, IC2 and IC5. Hence, the tensile strength ranges between 0.8 and 1.6 MPa, based on the FLAC3D modelling.

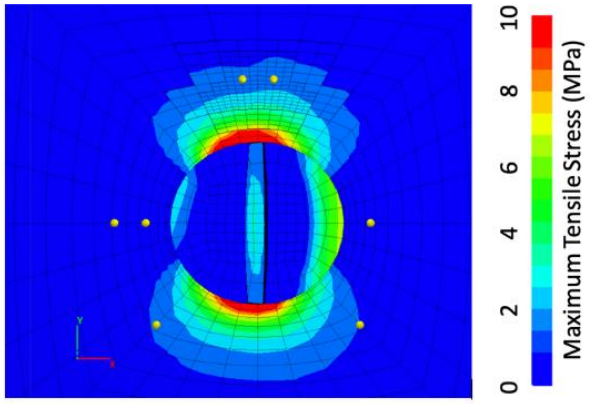

Figure 15. Tensile stresses at maximum load the response

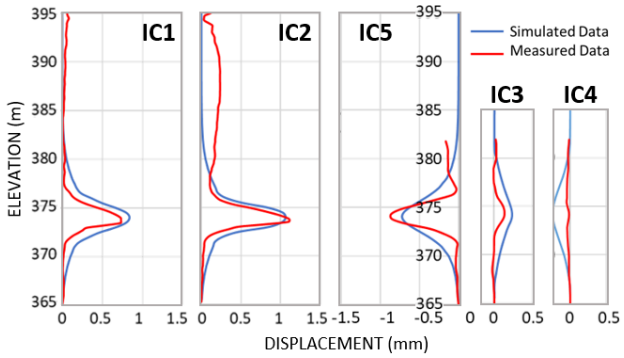

Figure 16. Displacement plots; c = 1.6 MPa, t = 0.8 MPa

6 CONCLUSION

The lateral load tests were successfully completed and clearly demonstrated that rock mass behaviour surrounding the 2.6-m diameter shaft remained essentially elastic at maximum loading. A three-dimensional numerical analysis was used to history-match the input parameters with the measured response. Based on these analyses, the following material parameters provided a model response that was in agreement with the measured response:

Isotropic Stiffness Parameters:

- Above El. 413 m: E = 4.3 GPa
- El. 413 m to 387 m: E increases from 4.3 to 6.6 GPa
- El. 387 m to 368 m: E increases from 6.6 to 22 GPa
- Below El. 368 m: E = 22 GPa

Rock mass Shear Strength Parameters:

- φ = 40° and c = 1.6 MPa

Tensile Strength:

- t > 0.8 MPa and <1.6 MPa

This set of parameters yielded a match to inclinometers IC1, IC2, and IC5 located on the active and passive sides along the assembly centerline. Lower stiffnesses and strengths in the back-analysis led to model displacements that were larger than the measured values.

The deformation modulus of the shale below the RCC was found to be approximately 18 to 22 GPa. These values are approximately 4 times greater than those reported for plate load tests carried out at El. 415 in the 1980 investigations.

7 ACKNOWLEDGEMENTS

The authors acknowledge the contributions to this project by Klohn Crippen Berger, SNC-Lavalin, Fugro Loadtest, the AFDE Partnership, Aecon Foundations, Dan Brown (Dan Brown Associates), the Site C Instrumentation and Geological team, Underhill Geomatics, and Foundex Explorations. The authors would also like to thank BC Hydro for permission to publish the results of the tests.

8 REFERENCES

Brown, D. A., Turner, J. P., Castelli, R. J., & Loehr, E. J. (2018). Drilled Shafts: Construction Procedures and LRFD Design Methods - GEC 10. *U.S. Department of Transportation Federal Highway Administration*, *FHWA-NHI 18-024*, 756p.

Conetec. (2020). BC Hydro Site-C Clean Energy Project, Results Of Pressuremeter Tests Carried Out By Cambridge Insitu Ltd.

Cornish, L. J., & Moore, D. P. (1985). *Dam foundation investigations for a project on soft shale*. Proceedings of 38th Canadian Geotechnical Conference, Edmonton, pp 171-178.

Hanna, A. and Little, T.E. 1992. An Estimate of Rebound Potential of the Shaftesbury Shales at a Dam Site in British Columbia, *Canadian Geotechnical Journal*, 29: 375-392.

Heidstra, N., Nunn, J., Watson, A.D., Dodman, K., Carter, R., and Burmeister, L. 2016. Roller Compacted Concrete Buttress at the Site C Clean Energy Project, *CDA 2016 Annual Conference, Bringing Dams into the Future*, 2016, Halifax, NS, Canada.

Imrie, A.S. 1991. Stress-induced Response from Both Natural and Construction-related Processes in the Deepening of the Peace River Valley, B.C., *Canadian Geotechnical Journal*, 28: 719-728.

Little, T.E. 1989. Construction and Performance of a Large Diameter Test Chamber in Shale, Proceedings of the International Congress on Progress and Innovation in Tunneling, 2: 869-876.

Sargent, D. W., & Cornish, L. J. (1985). *Water susceptibility of Shaftesbury shale*. Proceedings from Proceedings of 38th Canadian Geotechnical Conference, Edmonton, pp 197-206.

Shuri, F.S., Driscoll, D.D., and Garner, S.J. 1985. Controlled Displacement-rate In Situ Shear Tests with Pore Pressure Measurements, *Canadian Geotechnical Journal*, 22: 136-142.

Watson, A.D, Stevenson, G.W., and Hanna A. 2019. Site C Clean Energy Project, Design Overview, *Proceedings of the 87th Annual Meeting of International Commission on Large Dams, Sustainable and Safe Dams Around the World*, 2019 Canadian Dam Association, Ottawa, ON, Canada, 2: 2574-2587.